energies

MDPI

Article

Thermal Calculations of Four-Row Plate-Fin and Tube Heat Exchanger Taking into Account Different Air-Side Correlations on Individual Rows of Tubes for Low Reynold Numbers

Mateusz Marcinkowski *, Dawid Taler, Jan Taler and Katarzyna Węglarz

Faculty of Environmental Engineering and Energy, Cracow University of Technology, 31-155 Cracow, Poland; dawid.taler@pk.edu.pl (D.T.); jan.taler@pk.edu.pl (J.T.); katarzyna.weglarz@doktorant.pk.edu.pl (K.W.)
* Correspondence: mateusz.marcinkowski@doktorant.pk.edu.pl

Abstract: Currently, when designing plate-fin and tube heat exchangers, only the average value of the heat transfer coefficient (HTC) is considered. However, each row of the heat exchanger (HEX) has different hydraulic–thermal characteristics. When the air velocity upstream of the HEX is lower than approximately 3 m/s, the exchanged heat flow rates at the first rows of tubes are higher than the average value for the entire HEX. The heat flow rate transferred in the first rows of tubes can reach up to 65% of the heat output of the entire exchanger. This article presents the method of determination of the individual correlations for the air-side Nusselt numbers on each row of tubes for a four-row finned HEX with continuous flat fins and round tubes in a staggered tube layout. The method was built based on CFD modelling using the numerical model of the designed HEX. Mass average temperatures for each row were simulated for over a dozen different airflow velocities from 0.3 m/s to 2.5 m/s. The correlations for the air-side Nusselt number on individual rows of tubes were determined using the least-squares method with a 95% confidence interval. The obtained correlations for the air-side Nusselt number on individual rows of tubes will enable the selection of the optimum number of tube rows for a given heat output of the HEX. The investment costs of the HEX can be reduced by decreasing the tube row number. Moreover, the operating costs of the HEX can also be lowered, as the air pressure losses on the HEX will be lower, which in turn enables the reduction in the air fan power.

Keywords: plate-fin and tube heat exchanger; air-side Nusselt number; different heat transfer coefficient in particular tube row; mathematical simulation; numerical simulation; CFD simulation

check for updates

Citation: Marcinkowski, M.; Taler, D.; Taler, J.; Węglarz, K. Thermal Calculations of Four-Row Plate-Fin and Tube Heat Exchanger Taking into Account Different Air-Side Correlations on Individual Rows of Tubes for Low Reynold Numbers. *Energies* **2021**, *14*, 6978. https://doi.org/10.3390/en14216978

Academic Editor: Artur Bartosik

Received: 27 September 2021
Accepted: 20 October 2021
Published: 25 October 2021

Publisher's Note: MDPI stays neutral with regard to jurisdictional claims in published maps and institutional affiliations.

Copyright: © 2021 by the authors. Licensee MDPI, Basel, Switzerland. This article is an open access article distributed under the terms and conditions of the Creative Commons Attribution (CC BY) license (https://creativecommons.org/licenses/by/4.0/).

1. Introduction

Plate and fin heat exchangers (PFTHEs) are complicated devices. Their construction, which involves cross thin metal sheets and tubes with different numbers of rows, different fin pitches, and tube sizes, causes complicated phenomena on the air- and/or water-side [1]. Each row in PFTHEs operates in a different way. Differences are caused by variations in air and water temperatures, airflow turbulence, or even air velocity. Those elements cause different HTCs in each row [2].

Performance characteristics of tube heat exchangers are most often determined experimentally. This is usually due to the high complexity of the systems studied. An example is the experimental testing of photovoltaic (PV) cells cooled by phase-change materials (PCM) [3]. Fouling phenomena in exchangers are also investigated experimentally. Ali et al. [4] investigated the influence of dust deposited on the surface of two types of PVs, monocrystalline silicon, and polycrystalline silicon modules. Experimental studies are also widely used to determine the flow and heat characteristics of finned tube heat exchangers. Heat transfer correlations are determined on the side of the flowing gas, which is usually air, in a wide range of Reynolds number variations [5]. Additionally, the effectiveness of various types of improvements in the design of heat exchangers, such as oval tubes [6], new

fin shapes, or guide vanes forming the air flow in the exchanger [5], is usually evaluated experimentally. Despite the high reliability of the obtained results, a disadvantage is the cost of experimental studies. To determine the experimental characteristics of an exchanger with a different number of rows, tubes, or different construction, it is necessary to build an experimental test facility equipped with a measuring apparatus and a computer data acquisition system. Moreover, the time and therefore costs of experimental investigations are high. Therefore, CFD modelling is increasingly used in the development of tubular cross-flow heat exchangers [7]. The influence of various innovations in the design of the exchanger is modelled in different ranges of Reynolds numbers on the air-side and on the fluid-side flowing inside the tube. Four round-convex strips were placed around the tube to enhance air-side heat transfer [8].

If the experimental testing cannot be fully replaced, then the experiment comes down to verification of a certain part of the results [9]. The CFD modelling gives us increased flexibility in the research and industry. This study shows the newly determined correlations of the air-side Nusselt number for the four-row PFTHE. Those correlations illustrate new functions to determine HTC in a particular row of PFTHE. Individual correlations can also change the way we look at the heat flow inside PFTHE.

Until recently, plenty of Nusselt number, Colburn factor, or HTC correlations were determined. However, the majority are referred to as average correlations. Some studies presented local HTCs and only a few of them showed results or determined Nusselt number correlations for a particular row in multi-row PFTHEs.

The first group of research overviews is about average HTCs in PFTHEs. Khan et al. [10] investigated twisted oval tube HEXs and designated the average Nusselt numbers and pressure drop correlations. Lindqvist et al. [11] conducted CFD research taking into account different tube bundle array angles. They also presented diagrams with the Colburn factors for low Reynold numbers. Łęcki et al. [12] presented a comparison between HTCs obtained using CFD simulation to the one calculated with VDI correlation for three-row inline PFTHE. Sadeghianjahromi et al. [13] determined HTCs and pressure drop factors of PFTHEs with different fin types and circular and flat tubes under dry and wet conditions. Elmekawy et al. [14] showed that attaching the splitter plates to the tubes could increase the Nusselt number and reduce the pressure drop. Okbaz et al. [15] presented different Colburn factors correlations for PFTHEs with different numbers of rows. However, those correlations were averaged for entire PFTHEs. Petrik and Szepesi [16] determined Nusselt number correlations for one and two-row U-shape HEXs. Additionally in another piece of research, Petrik et al. [17] presented Nusselt number correlations but for standard PFTHEs. González et al. [18] presented the average Nusselt numbers as a function of fin material and Reynolds number for two-row PFTHE with inline tube arrangement. Awais and Bhuiyan [19] collected plenty of Colburn factor correlations in their state-of-the art paper. It is possible to present many more average correlations. However, it is not necessary for this research. Adam et al. [20], in a state-of-the-art paper, shows studies of local HTCs and local heat/mass transfers coefficients.

All of the above research is related to the average Nusselt numbers, Colburn factors, or HTC correlations, or presents local HTCs to predict heat transfer correlations for the entire PFTHE. There are only a couple instances of research referring to heat transfer correlations for a particular row in PFTHEs. During the 1970s, Rich et al. [21] showed experimental research where a Colburn factor in a particular row for multi-row PFTHEs, with one-row to eight-rows, was presented. This was the first time when someone showed variation in the HTC inside PFTHEs. Taler et al. [2] determined individual Nusselt number correlations for each row in the case of two-row PFTHE. Despite its high practical importance and current marginal existence in the literature, there is a lack of heat transfer correlations on individual tube rows for heat exchangers with different number of tube rows. Additionally, the literature is full of average Nusselt number, Colburn factor, or HTC correlations for different fin geometries, tube geometries, fin pitches, tube sizes, air velocities, etc.

Only Rich et al. [21] showed that further tube rows in multi-row PFTHEs are inefficient when the air velocity is low and the airflow in the exchanger is laminar. However, correlations on Nusselt number for individual tube rows have not been developed. Taler et al. [22] showed that in a two-row automotive radiator, made with round or oval tubes, the first row of tubes is more efficient than the second row when the air velocity is less than 2.5 m/s. However, coolers with larger tube numbers have not been modelled by CFD or studied experimentally. There are many problems to solve, such as: whether a larger cross-section of a PFTHE, but with a smaller number of rows, would be more efficient than a three-, four-, or five-row PFTHE. Which row is the least effective? Should we consider individual correlations in the case of multi-row PFTHEs?

The present research refers to four-row PFTHE with the air velocity before the HEX changing in the range from 0.5 m/s to 2.5 m/s. This paper covers:

- Determination of individual air-side Nusselt number correlations by CFD simulation;
- Determination of average air-side Nusselt number correlations by CFD simulation;
- Comparison of determined correlations to correlations available in the literature.

2. Problem Statement

This paper presents a three-dimensional (3D) steady-state CDF simulation of PFTHE under the following assumptions:

- Constant air inlet temperature: 20 °C.
- Air outlet as an open condition with checking the average mass temperature in the air outlet cross-section.
- Constant air-side wall surface temperature (including tube and fins temperature): 70 °C.
- Variable air parameters dependent on the temperature.
- Shear Stress Transport (SST) turbulence model.
- Relative differences (e_{T_n}) between different mass average air temperatures in the last (the fourth) row of PFTHE for mesh with particular element numbers (T_{ni}) and the reference mass average temperature in the last (the fourth) row of PFTHE for mesh with 6,790,572 mesh elements ($T_{6,790,572}$) are shown in Equation (1). The above reference mesh has been selected for further calculations as the best ratio of calculation accuracy to calculation time.

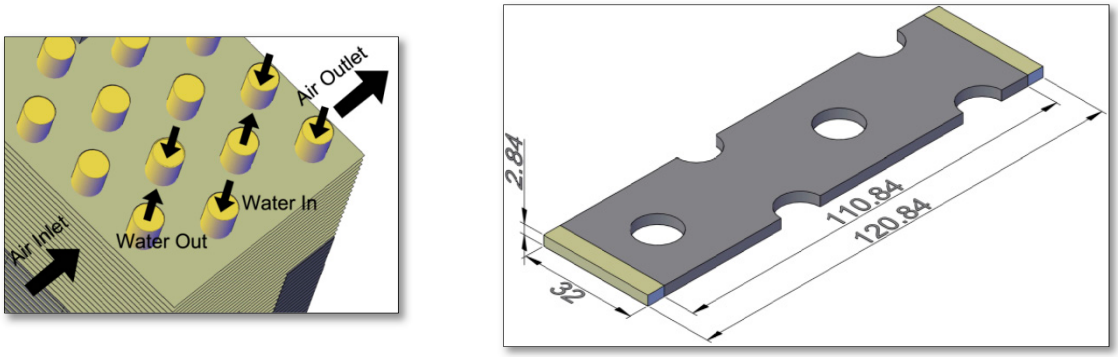
$$e_{T_n} = \frac{(T_{ni} - T_{6,790,572})}{T_{6,790,572}} \quad (1)$$

- Relative differences (e_{T_w}) between the Nusselt number for a particular fin and tube surface temperature (Nu_{T_w}) and Nusselt number for the reference fin and tube surface temperature: 70 °C ($Nu_{70\ ^\circ C}$) as calculated according to Equation (2).

$$e_{T_w} = \frac{(Nu_{T_w} - Nu_{70\ ^\circ C})}{Nu_{70\ ^\circ C}} \quad (2)$$

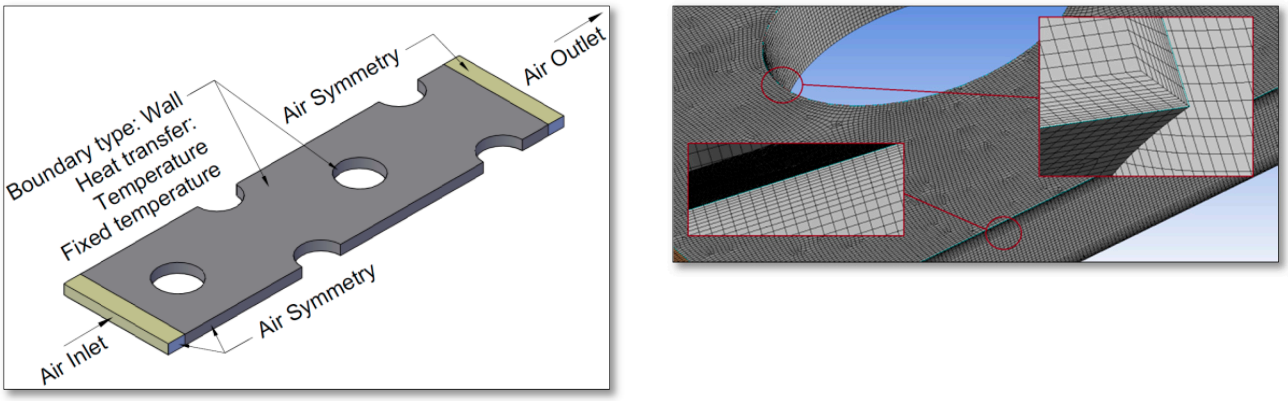
3. Description of the Geometry of the Repeating Element of the Exchanger

Figure 1 presents a 3D view and geometry of analysed PFTHE. Directions of air and water flow are shown. Figure 1b illustrates a repetitive fragment of air between one fin pitch in PFTHE (grey colour). In this case, fin pitch equals 3 mm. However, the distance between surfaces of the adjacent plate fins is 2.84 mm. This is because the fin thickness is 0.14 mm. In the same picture, we can observe yellow colours in front and behind the PFTHE. Those fragments are free zones of air for the correct performance of CFD simulation. Each zone is 5 mm in length (Figure 1b). The diameter of the tubes is 12mm. Air Inlet in CFX software is set as a constant temperature: 20 °C. Air outlet is set as an opening condition with checking mass average temperature in the outlet cross section of air. The rest of the boundary conditions of the CFX software are shown in Figure 2a.



(**a**) (**b**)

Figure 1. (**a**) The analysed PFTHE: 3D view; (**b**) Repetitive fragment of the PFTHE with run-up zone using in ANSYS-CFX 2020 R2: geometry, mm.



(**a**) (**b**)

Figure 2. Repetitive fragment of the PFTHE with run-up zone using in ANSYS-CFX 2020 R2: (**a**) boundary conditions; (**b**) finite element mesh.

4. Mesh Parameters and Mesh Independent Study

Mesh characteristics are presented in Table 1. The division of the modelled domain into finite elements considers mesh compaction at the junction of the air and fin wall surface and air and tube wall surface (Figure 2b).

Table 1. Specification of the finite element mesh for the model presented in Figure 2b.

Number of Finite Elements	6,790,572
Number of nodes	6,989,646
The dimension of the element, mm	0.15
The maximal dimension of the element, mm	0.25
Boundary layer	First layer thickness: 0.023 mm $(y^+ = 1)$ Growth rate: 1.1 Number of layers: 12
Minimum orthogonal angle	Air: 36°
Mesh expansion factor	Air: 12
Maximum aspect ratio	Air: 20

All simulations for the entire range of air velocity were preceded by mesh independent studies, separately for all considered air velocities. The final mesh was selected only for the most favourable simulation. Temperature stabilisation for air velocity—4 m/s for the

fourth row of PFTHE—is shown in Figure 3. It was observed that, from air velocity in front of PFTHE, more than 2.5 m/s temperature stabilisation is not much different in comparison with temperature stabilisation in the fourth (last) row of PFTHE. Temperature stabilisation showed that, between chosen mesh element size and mesh with almost 30 million elements, relative differences were less than 1% for the fourth row of PFTHE (Figure 3). Moreover, for the first row, even for 10 m/s relative differences between chosen mesh and mesh with over 30 million, elements are less than 0.1% (Equation (1). This shows that, in the considered scenario, the greatest irregularity of flow and turbulence exists in the last row of PFTHE.

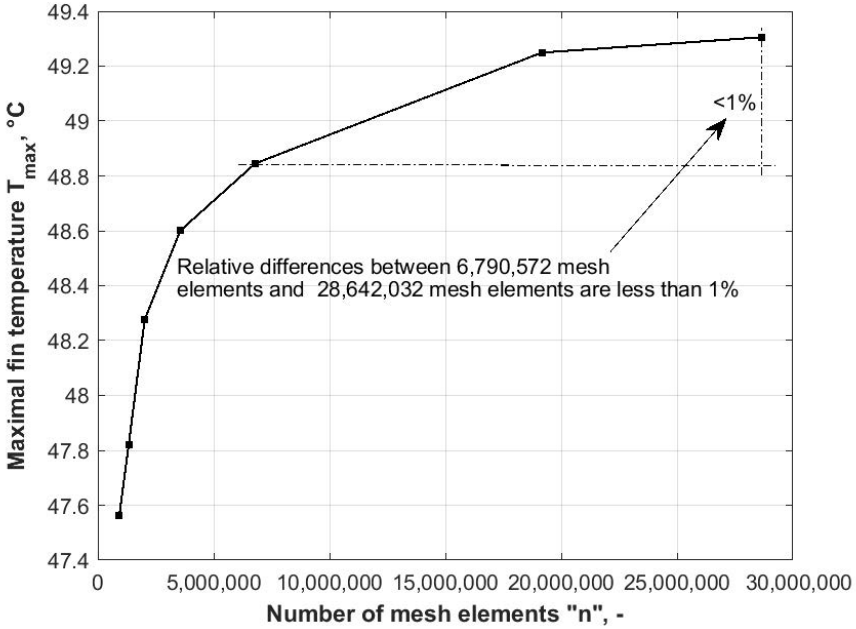


Figure 3. Temperature stabilisation for mesh independent study from the fourth row of PFTHE for 4 m/s air velocity in front of the heat exchanger.

A mesh with 6,790,572 elements was selected. Mesh elements' size belongs to the following CFX mesh sizes: mesh element size: 0.15 mm; mesh max size: 0.25 mm (Table 1). The whole mesh contains cuboidal elements only (Figure 1b).

5. Method of Determining HTC on the Individual Row Based on CFD Simulations

A method for determining HTCs for the individual rows is illustrated with an example of four-row PFTHE (Figure 4). The HTC is appointed, factoring constant fin and tube temperatures, which are equal to 70 °C Further simulations have also been performed for two different temperatures: 60 °C and 80 °C. It has been shown that, for three different surface temperatures of the tubes and fins, the determined HTCs do not differ more than 1.5% (Figure 5), and that proposed procedure for determining the air-side HTC can be successfully used in practice. The method consists of the following steps.

- Export the average mass flow temperature $\overline{T}^i{}_a$ from CFX simulations of considered air velocity ranging for each row independently. Cross-section to export temperatures in a half distance between the next two tubes in rows.
- Calculate the mean logarithmic temperature ($\Delta\overline{T}_{m,a}$) difference between fin and tube surface temperature (T_w) and average mass flow temperature ($\overline{T}^i_a$) (Equation (3).

$$\Delta T^i_{m,a} = \frac{\left(T_w - \overline{T}^{i+1}_a\right)\left(T_w - \overline{T}^i_a\right)}{ln\left(\frac{T_w - \overline{T}^{i+1}_a}{T_w - \overline{T}^i_a}\right)} \quad (3)$$

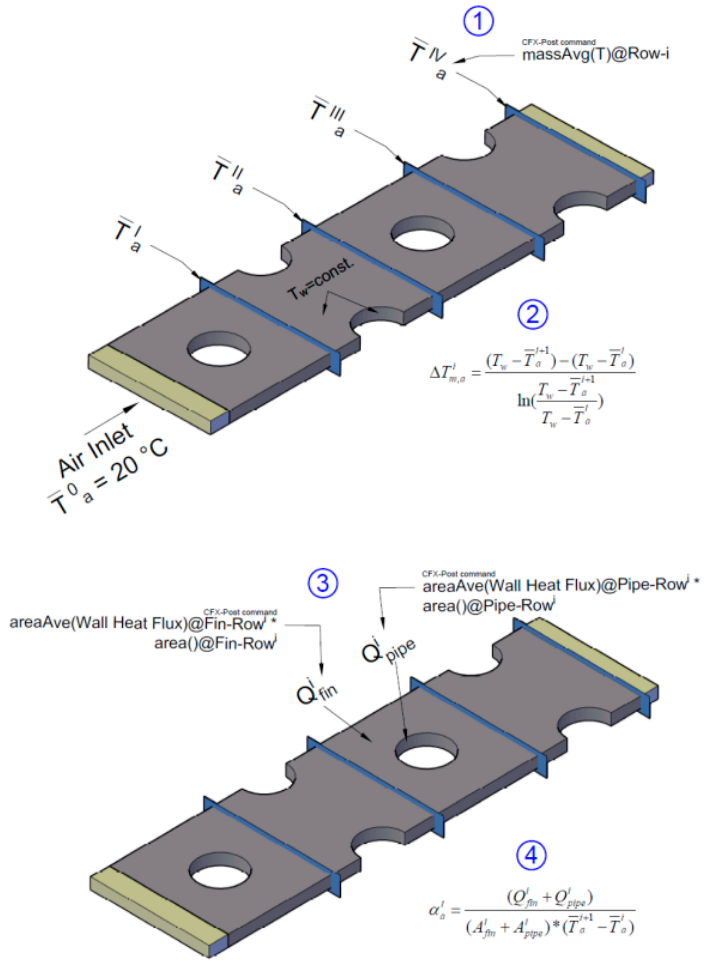


Figure 4. Graphical representation of determining HTC on the individual row based on a CFD simulation. The numbers on the picture show the order of calculation to determine HTC in the case of PFTHE.

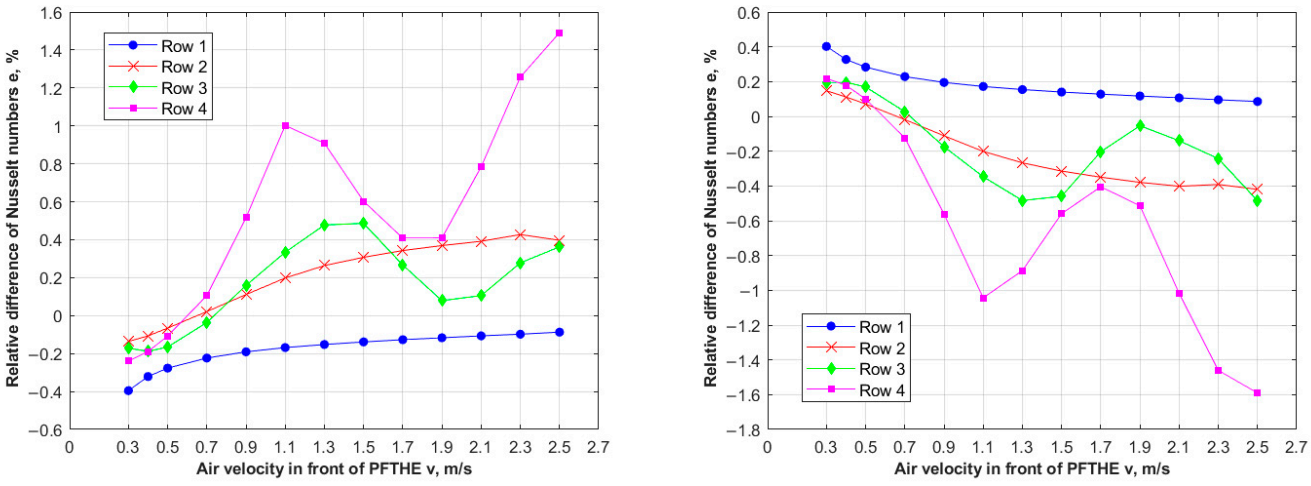


Figure 5. Relative differences of Nusselt numbers for each row of PFTHE for different air wall temperatures (constant temperature of fin and tube wall), where reference temperature is 70 °C: (**a**) 70 °C and 80 °C; (**b**) 70 °C and 60 °C.

The symbol T_w denotes a constant fin and tube surface temperature. The symbols $\overline{T}_a^i$ and $\overline{T}_a^{i+1}$ designate the inlet and outlet mass average air temperature for the i-th row of PFTHE. Then:

- Export total heat flow rate transferred from fin and tube wall surface to air (Figure 4).
- Calculate individual HTC for each row (Equation (4) (Figure 4)).

$$\alpha_a^i = Q_i / \left(A_w \Delta T_{m,a}^i \right) \tag{4}$$

The following designations are used in Equation (4): Q_i the total heat flow rate for the entire row of the repetitive fragment of PFTHE; α_a^i the air-side HTC in a particular row.

- Calculate Nusselt number $Nu_a^i = (\alpha_a^i \, d_h)/\lambda_a$ and Colburn factor $j_a^i = Nu_a^i / \left(Re_a^i \, Pr_a^{i\,1/3} \right)$.

6. CFD Simulation Results and Nusselt Number Correlations

The CFD simulation results of average mass flow temperatures behind the tube rows are shown in Table 2.

Table 2. CFD simulation data.

i	$w_{o,i}$, m/s	$T^I_{a,i}$, °C	$T^{II}_{a,i}$, °C	$T^{III}_{a,i}$, °C	$T^{IV}_{a,i}$, °C
1	0.3	59.95	67.67	69.42	69.85
2	0.4	55.55	65.13	68.23	69.34
3	0.5	52.06	62.51	66.62	68.44
4	0.7	47.07	57.91	63.10	66.03
5	0.9	43.72	54.37	59.97	63.59
6	1.1	41.33	51.69	57.45	61.63
7	1.3	39.53	49.60	55.46	60.08
8	1.5	38.11	47.94	53.87	58.71
9	1.7	36.96	46.57	52.51	57.43
10	1.9	36.01	45.41	51.27	56.25
11	2.1	35.21	44.41	50.17	55.21
12	2.3	34.52	43.54	49.21	54.34
13	2.5	33.92	42.76	48.35	53.58

Presented correlations for air-side Nusselt numbers relate to Reynolds numbers. The Reynolds number (Equation (5) is related to the hydraulic diameter, which is calculated using the definition proposed by Kays and London [23], where w_{max} is given by Equation (6). Parameter w_{max} has been calculated for the minimum airflow cross-section between tubes and it can exist in a different place in case of different PFTHE construction. The hydraulic diameter has been calculated by assumption dividing the volume through which air flows in one row by the surface area in contact with the air. Most often, this hydraulic diameter in the case of PFTHE is a bit smaller than double the fin pitch, and using geometry from Figure 1, equals 5.35 mm.

Reynolds numbers ($Re_{d_h,a}$) (Equation (5) and maximal velocities (w_{max}) (Equation (6)) have been calculated for each row separately, due to a different maximum air velocity caused by higher air temperature causing increased air volume. The calculated parameters such as Reynolds numbers, HTCs, Nusselt numbers, and Colburn factors are presented in Tables 3–6.

$$Re_{d_h,a} = \frac{w_{max} \cdot d_h}{\nu_a} \tag{5}$$

Table 3. Calculated thermal parameters for the first row of PFTHE.

i	$w_{o,i}$, m/s	$w_{max,i}$, m/s	$Re^{I}_{a,i}$	$\alpha^{I}_{a,i}$	$Nu^{I}_{a,i}$	$j^{I}_{a,i}$
1	0.3	0.54	169.6	17.07	3.33	0.022647
2	0.4	0.71	227.4	17.57	3.45	0.017474
3	0.5	0.89	285.4	18.14	3.58	0.014413
4	0.7	1.23	402.0	19.32	3.84	0.010949
5	0.9	1.57	519.1	20.53	4.09	0.009035
6	1.1	1.91	636.3	21.72	4.35	0.007813
7	1.3	2.25	753.7	22.89	4.59	0.006959
8	1.5	2.60	871.2	24.02	4.83	0.006325
9	1.7	2.94	988.7	25.12	5.06	0.005832
10	1.9	3.28	1106.4	26.19	5.28	0.005437
11	2.1	3.62	1224.1	27.22	5.49	0.005112
12	2.3	3.96	1341.8	28.24	5.70	0.004839
13	2.5	4.30	1459.6	29.22	5.91	0.004606

Table 4. Calculated thermal parameters for the second row of PFTHE.

i	$w_{o,i}$, m/s	$w_{max,i}$, m/s	$Re^{II}_{a,i}$	$\alpha^{II}_{a,i}$	$Nu^{II}_{a,i}$	$j^{II}_{a,i}$
1	0.3	0.54	150.9	15.44	2.83	0.021261
2	0.4	0.72	204.1	15.31	2.83	0.015750
3	0.5	0.90	258.2	15.35	2.86	0.012582
4	0.7	1.25	368.2	15.74	2.97	0.009166
5	0.9	1.60	479.6	16.44	3.13	0.007413
6	1.1	1.95	591.8	17.34	3.32	0.006379
7	1.3	2.29	704.6	18.38	3.54	0.005708
8	1.5	2.64	817.7	19.49	3.77	0.005234
9	1.7	2.98	931.2	20.61	4.00	0.004876
10	1.9	3.33	1044.9	21.73	4.23	0.004593
11	2.1	3.67	1158.9	22.83	4.45	0.004360
12	2.3	4.02	1273.0	23.90	4.67	0.004165
13	2.5	4.36	1387.4	24.93	4.88	0.003992

Table 5. Calculated thermal parameters for the third row of PFTHE.

i	$w_{o,i}$, m/s	$w_{max,i}$, m/s	$Re^{III}_{a,i}$	$\alpha^{III}_{a,i}$	$Nu^{III}_{a,i}$	$j^{III}_{a,i}$
1	0.3	0.55	147.6	14.62	2.65	0.020270
2	0.4	0.73	198.3	14.23	2.59	0.014768
3	0.5	0.91	250.0	13.97	2.55	0.011563
4	0.7	1.26	355.6	13.78	2.55	0.008108
5	0.9	1.61	463.1	14.02	2.61	0.006391
6	1.1	1.96	571.7	14.60	2.74	0.005429
7	1.3	2.31	680.9	15.47	2.92	0.004856
8	1.5	2.66	790.6	16.54	3.13	0.004491
9	1.7	3.01	900.7	17.52	3.33	0.004191
10	1.9	3.36	1011.3	18.26	3.48	0.003902
11	2.1	3.71	1122.2	18.91	3.62	0.003652
12	2.3	4.05	1233.3	19.60	3.76	0.003452
13	2.5	4.40	1344.8	20.29	3.90	0.003284

Table 6. Calculated thermal parameters for the first row of PFTHE.

i	$w_{o,i}$, m/s	$w_{max,i}$, m/s	$Re^{IV}{}_{a,i}$	$\alpha^{IV}{}_{a,i}$	$Nu^{IV}{}_{a,i}$	$j^{IV}{}_{a,i}$
1	0.3	0.55	146.9	14.34	2.59	0.019199
2	0.4	0.73	196.5	13.92	2.52	0.013971
3	0.5	0.91	246.9	13.70	2.49	0.010986
4	0.7	1.27	349.7	13.71	2.51	0.007826
5	0.9	1.62	454.5	14.33	2.64	0.006350
6	1.1	1.98	560.4	15.88	2.94	0.005743
7	1.3	2.33	666.9	17.73	3.30	0.005419
8	1.5	2.68	773.9	19.11	3.57	0.005055
9	1.7	3.04	881.5	20.14	3.77	0.004694
10	1.9	3.39	989.8	21.06	3.96	0.004389
11	2.1	3.74	1098.5	22.11	4.17	0.004165
12	2.3	4.09	1207.4	23.45	4.43	0.004030
13	2.5	4.44	1316.6	24.93	4.72	0.003939

The following designations are used in Equation (5): $Re_{d_h,a}$ is the Reynolds number in case of air hydraulic diameter; d_h is the air hydraulic diameter; ν_a is the air kinematic viscosity.

$$w_{max} = \frac{(s \cdot p_l)}{\left(s - \delta_f\right) \cdot (p_l - d_{o,min})} \cdot \frac{\left(\overline{T}_a^i\right)}{\left(\overline{T}_{a,o}\right)} \cdot w_o \tag{6}$$

The symbol w_{max} designates the air velocity in the least cross-section of the air flow. The symbol s denotes fin pitch. Other symbols represent: p_l the longitudinal fin pitch δ_f the fin thickness, $d_{o,min}$ the minimal dimension between tubes, $\overline{T}_a^i$ the mass average air temperature in i-th row of PFTHE, and $\overline{T}_{a,o}$ the inlet mass average air temperature.

The approximation function was determined using the least-squares method. Using this function, the Nusselt number was approximated, depending on the Reynolds and Prandtl numbers, according to Equation (7). The range of Reynolds numbers considered is factored in the present study, and is also present in Equation (7).

$$Nu_a = x_1 \cdot Re^{x_2} \cdot Pr^{\frac{1}{3}} \qquad 140 < Re < 1500 \tag{7}$$

The heat transfer correlation for the entire heat exchanger is shown in Figure 6. The Nusselt numbers for the first and second rows of tubes as a function of the Reynolds number, calculated separately for each row, are illustrated in Figure 7a,b. The heat transfer correlations for the third and fourth rows of tubes are shown in Figure 8a,b. Figures 6–8 also show the confidence intervals for the Nusselt number calculated using Equation (7). The legend of each figure shows the corresponding correlation, either for the whole exchanger (Figure 6) or for a given row of tubes (Figures 7 and 8). Each figure also shows the limits of the 95% confidence intervals for the Nusselt number on a given tube row, where the coefficients x_1 and x_2 are determined by the least-squares method. For the 95% confidence interval, the values of the Nusselt number calculated for a given Reynolds number (Equation (7)) differ by $+/-2\,\sigma$, where the symbol σ denotes the mean standard deviation of the Nusselt numbers obtained by the CFD modelling. The process of determining 95% confidence intervals for correlations per Nusselt number obtained by least-squares is detailed in Chapter 11 of Taler's book [24].

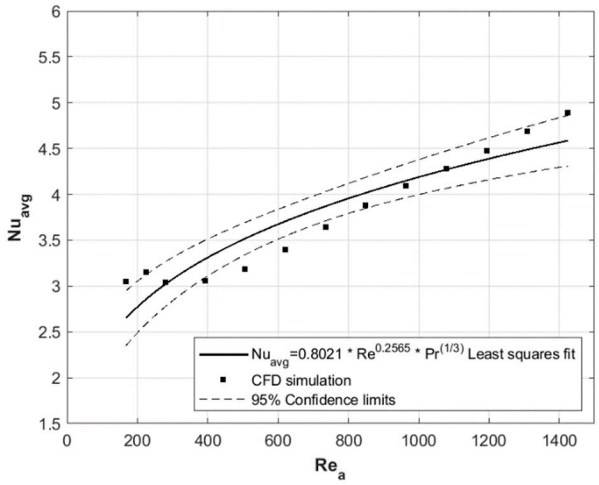
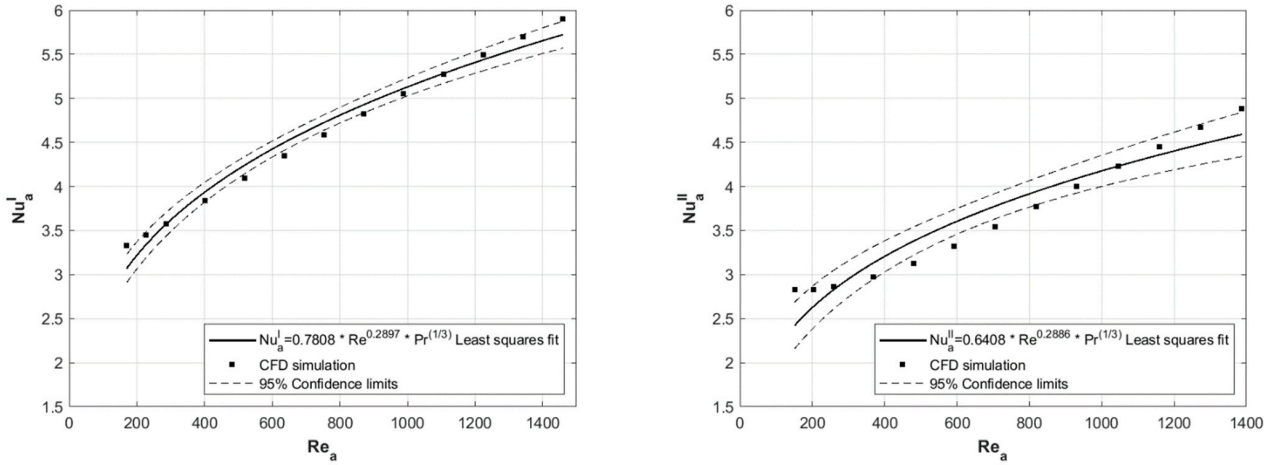
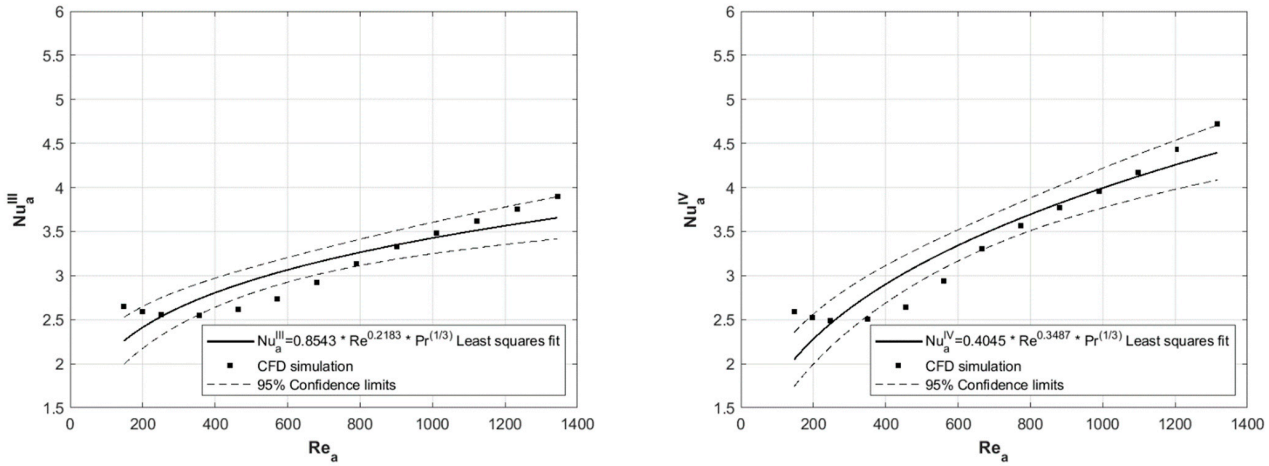


Figure 6. The average value of the Nusselt number as a function of the Reynolds number for the entire PFTHE.



(**a**) (**b**)

Figure 7. The Nusselt number as a function of the Reynolds number: (**a**) for the first row of PFTHE; (**b**) for the second row of PFTHE.



(**a**) (**b**)

Figure 8. The Nusselt number as a function of the Reynolds number: (**a**) for the third row of PFTHE; (**b**) for the fourth row of PFTHE.

7. Discussion of the Obtained Results

Nusselt number correlations for considered PFTHE (Figure 1) have been determined using the CFD simulation data. New individual correlations (Figures 7 and 8) for particular rows are significantly different from the average Nusselt number correlation for the entire PFTHE (Figure 6), also determined by the CFD simulation. Parameter x_2 in Equation (7) determined by the least-squares method is compatible only for the first row with parameters known in the literature [2], while in the second row, there is a 46% discrepancy compared to the parameter x_2 found by [2] for the two-row car radiator. The heat transfer correlations for the last two rows, the third, and fourth, are new and there are no existing correlations in the literature for comparison.

Additionally, Nusselt numbers fall between Reynolds numbers from 140 to 500, although they also increase from 500 to 1400. This increase may occur when the air stream does not separate away from the tube for low air velocity (0.3 m/s). The Nusselt number value is larger for higher air velocity (0.5 m/s–0.7 m/s) where the detachment of the air stream from the tube surface occurs.

The determined heat transfer correlations showed that the third row is the least efficient. It has been noticed that, for the entire air velocity range, the Nusselt number falls to the third row and then increases in the fourth row. This could mean that airflow in the penultimate row is less turbulent or airflow has formed only a narrow flow channel, leaving a wide heat transfer dead zone in front of and behind the tubes in the third row.

Experimental verification of derived CFD-based correlations has not been carried out in this paper. Experimental verification is planned as an extension of this research. The future of this research topic also considers a wider Reynolds number range, different tube and fin pitches, and tube diameters of PFTHE.

8. Conclusions

New heat transfer correlations for the air-side Nusselt number have been proposed for four-row PFTHE. Consideration of individual correlations on individual rows of heat exchanger tubes can improve designing of the PFTHEs. In the analysed range of air velocities in front of the heat exchanger from 0.3 m/s to 2.5 m/s, the average HTC for the first tube row has the highest value. In the subsequent tube rows, the HTC is lower compared to the HTC on the first tube row. This paper also presents a simple method for the determination of Nusselt number correlation for individual rows, which can reduce or even eliminate experimental research. The adoption of a constant external surface temperature for the ribs and tubes simplifies the determination of HTC on individual tube rows. It is shown that, for constant fin and tube surface temperatures of 60 °C, 70 °C, and 80 °C, the resulting HTC values for the same airflow velocity differ slightly. However, CFD simulation must be precisely conducted with a proper finite volume mesh and turbulence model for turbulent flows. CFD modelling is an effective tool for determining individual correlations for calculating the air-side Nusselt number on the individual tube rows of the exchanger.

Author Contributions: Conceptualisation, D.T., J.T.; methodology, software, validation, formal analysis, investigation, writing—original draft preparation, M.M.; resources, data curation, M.M., K.W.; writing—review and editing; supervision, D.T., J.T. All authors have read and agreed to the published version of the manuscript.

Funding: This research received no external funding.

Institutional Review Board Statement: Not applicable.

Informed Consent Statement: Not applicable.

Data Availability Statement: The data presented in this study are available on request from the corresponding authors.

Conflicts of Interest: The authors declare no conflict of interest.

Nomenclature

A_{fin}	area of the fin sides, m^2
A_{tube}	tube outer surface area, m^2
d_h	hydraulic diameter, m
d_o	tube outer diameter, m
e	relative differences, %
j	Colburn factor
n	number of mesh elements
Nu	Nusselt number
p_l	longitudinal fin pitch, m
p_t	transversal fin pitch, m
Pr	Prandl number
r_{in}	outer radius of a plain tube, m
s	fin pitch, m
Re	Reynold number
$\overline{T}_a$	mass average air temperature, °C
$\overline{T}_{a,0}$	air inlet temperature, °C
$\Delta\overline{T}_{m,a}$	log mean temperature difference, °C
T_w	wall temperature (tube and fin), °C
w	air velocity, m/s
Q	total heat transfer rate, W
x_1	Nusselt number parameter
x_2	Nusselt number parameter
y^+	dimensionless wall distance
α	heat transfer coefficient, $W/(m^2.K)$
λ	thermal conductivity coefficient, W/(m.K)
δ_f	fin thickness, m
σ	standard deviation
ν	air kinematic viscosity, m^2/s
0, I, II, III, IV	number of PFTHE row
i	current row of PFTHE
i+1	next row of PFTHE
a	air
avg	average
i	next iteration
max	maximal

References

1. Thulukkanam, K. *Heat Exchanger Design Handbook*, 2nd ed.; CRC Press: Boca Raton, FL, USA, 2013.
2. Taler, D.; Taler, J.; Trojan, M. Thermal calculations of plate–fin–and-tube heat exchangers with different heat transfer coefficients on each tube row. *Energy* **2020**, *203*, 117806. [CrossRef]
3. Ali, H.M. Recent advancements in PV cooling and efficiency enhancement integrating phase change materials based systems—A comprehensive review. *Sol. Energy* **2020**, *197*, 163–198. [CrossRef]
4. Ali, H.M.; Zafar, M.A.; Bashir, M.A.; Nasir, M.A.; Ali, M.; Siddiqui, A.M. Effect of dust deposition on the performance of photovoltaic modules in city of taxila, Pakistan. *Therm. Sci.* **2017**, *21*, 915–923. [CrossRef]
5. Li, X.Y.; Li, Z.H.; Tao, W.Q. Experimental study on heat transfer and pressure drop characteristics of fin-and-tube surface with four convex-strips around each tube. *Int. J. Heat Mass Transf.* **2018**, *116*, 1085–1095. [CrossRef]
6. Matos, R.S.; Vargas, J.V.C.; Rossetim, M.A.; Pereira, M.V.A.; Pitz, D.B.; Ordonez, J.C. Performance comparison of tube and plate-fin circular and elliptic heat exchangers for HVAC-R systems. *Appl. Therm. Eng.* **2021**, *184*, 116288. [CrossRef]
7. Maarawi, A.; Anxionnaz-Minvielle, Z.; Coste, P.; Raimondi, N.D.M.; Cabassud, M. 1D/3D Numerical Approach for Modelling a Milli-Structured Heat Exchanger/Reactor. *Chem. Eng. Trans.* **2021**, *86*, 1441–1446.
8. Li, X.Y.; Mu, Y.T.; Li, Z.H.; Tao, W.Q. Numerical study on the heat transfer and pressure drop characteristics of fin-and-tube surface with four round-convex strips around each tube. *Int. J. Heat Mass Transf.* **2020**, *158*, 120034. [CrossRef]
9. Marcinkowski, M.; Taler, D. Calculating the Efficiency of Complex-Shaped Fins. *Energies* **2021**, *14*, 577. [CrossRef]
10. Khan, M.S.; Zou, R.; Yu, A. Computational simulation of air-side heat transfer and pressure drop performance in staggered mannered twisted oval tube bundle operating in crossflow. *Int. J. Therm. Sci.* **2021**, *161*, 106748. [CrossRef]

11. Lindqvist, K.; Skaugen, G.; Meyer, O.H.H. Plate fin-and-tube heat exchanger computational fluid dynamics model. *Appl. Therm. Eng.* **2021**, *189*, 116669. [CrossRef]
12. Łęcki, M.; Andrzejewski, D.; Gutkowski, A.N.; Górecki, G. Study of the Influence of the Lack of Contact in Plate and Fin and Tube Heat Exchanger on Heat Transfer Efficiency under Periodic Flow Conditions. *Energies* **2021**, *14*, 3779. [CrossRef]
13. Sadeghianjahromi, A.; Wang, C.C. Heat transfer enhancement in fin-and-tube heat exchangers—A review on different mechanisms. *Renew. Sustain. Energy Rev.* **2021**, *137*, 110470. [CrossRef]
14. Elmekawy, A.M.N.; Ibrahim, A.A.; Shahin, A.M.; Al-Ali, S.; Hassan, G.E. Performance enhancement for tube bank staggered configuration heat exchanger—CFD Study. *Chem. Eng. Process.-Process Intensif.* **2021**, *164*, 108392. [CrossRef]
15. Okbaz, A.; Pınarbaşı, A.; Olcay, A.B. Experimental investigation of effect of different tube row-numbers, fin pitches and operating conditions on thermal and hydraulic performances of louvered and wavy finned heat exchangers. *Int. J. Therm. Sci.* **2020**, *151*, 106256. [CrossRef]
16. Petrik, M.; Szepesi, G. Experimental and numerical investigation of the air side heat transfer of a finned tubes heat exchanger. *Processes* **2020**, *8*, 773. [CrossRef]
17. Petrik, M.; Szepesi, G.; Jármai, K. CFD analysis and heat transfer characteristics of finned tube heat exchangers. *Pollack Period.* **2019**, *14*, 165–176. [CrossRef]
18. González, A.M.; Vaz, M.; Zdanski, P.S.B. A hybrid numerical-experimental analysis of heat transfer by forced convection in plate-finned heat exchangers. *Appl. Therm. Eng.* **2019**, *148*, 363–370. [CrossRef]
19. Awais, M.; Bhuiyan, A.A. Heat and mass transfer for compact heat exchanger (CHXs) design: A state-of-the-art review. *Int. J. Heat Mass Transf.* **2018**, *127*, 359–380. [CrossRef]
20. Adam, A.Y.; Oumer, A.N.; Najafi, G.; Ishak, M.; Firdaus, M.; Aklilu, T.B. State of the art on flow and heat transfer performance of compact fin-and-tube heat exchangers. *J. Therm. Anal. Calorim.* **2020**, *139*, 2739–2768. [CrossRef]
21. Rich, D. The effect of the number of tube rows on heat transfer performance of smooth plate fin-and-tube heat exchangers. *ASHRAE Trans.* **1975**, *81*, 307–317.
22. Taler, D.; Taler, J.; Trojan, M. Experimental verification of an analytical mathematical model of a round or oval tube two-row car radiator. *Energies* **2020**, *13*, 3399. [CrossRef]
23. Kays, W.; London, A. *Compact Heat Exchangers*, 3rd ed.; Krieger Pub Co.: Malabar, FL, USA, 1998.
24. Taler, D. *Numerical Modelling and Experimental Testing of Heat Exchangers*; Springer Nature: Cham, Switzerland, 2019.